Peer reviewed version

Link to published version (if available):
10.2514/6.2021-1153

Link to publication record in Explore Bristol Research
PDF-document

University of Bristol - Explore Bristol Research
General rights

Folding Wingtips for Improved Roll Performance

Fintan Healy*, Ronald Cheung [†], Theodor Neofet[‡], Mark Lowenberg[§], Djamel Rezgui[¶] and Jonathan Cooper [∥]
University of Bristol, Bristol, BS81TR, UK

Andrea Castrichini** and Tom Wilson[††]
Airbus Operations Ltd, Bristol, BS34 7QQ, UK

Future aircraft designs look set to use longer wing spans to increase the aspect ratio and therefore overall aerodynamic efficiency of the airframe. Such larger wing spans also reduce roll rates and require increased control surface area to achieve the roll maneuver requirements for certification. In this work, the effect of using flared folding wingtips (FFWTs) on the roll performance of simple aircraft wings is investigated numerically and experimentally. A unique rolling rig is designed, manufactured and tested, with a series of steady roll and transient tests performed for different wing spans, with and without folding wingtips. It is shown that the use of FFWTs on aircraft wings can enable improved aerodynamic performance due to the increased span whilst also significantly reducing the aerodynamic damping due to roll, such that the roll performance of a wing incorporating FFWTs is comparable to that of one without the additional span.

Nomenclature

Greek Symbols

α	=	angle of attack
β	=	aileron angle
θ	=	fold angle
Λ	=	flare angle
ρ	=	air density
σ	=	folding wingtip span as a ratio of the semi-span
τ	=	torque
ϕ	=	roll angle

Roman Symbols

c	=	chord
C_{β}	=	control surface torque coefficient
f, g	=	generic functions
l	=	moment arm
m	=	mass
M	=	mass matrix
p	=	roll rate
q	=	generalised coordinates
s	=	wing span
V	=	velocity
w	=	vertical velocity component

---

*PhD Student, Department of Aerospace Engineering.

[†]Research Associate, Department of Aerospace Engineering.

[‡]MEng Student, Department of Aerospace Engineering.

[§]Professor of Flight Mechanics, Department of Aerospace Engineering, SMAIAA.

[¶]Senior Lecturer, Department of Aerospace Engineering MAIAA.

[∥]Airbus RAEng Sir George White Professor of Aerospace Engineering, Department of Aerospace Engineering, FAIAA

**Loads and Aeroelastics Engineer.

[††]Loads and Aeroelastics Expert.

| y | = | spanwise coordinate |

Subscripts

a	=	due to aerodynamic forces
c	=	due to centrifugal forces
i	=	induced by the rolling motion
f	=	of the folding wingtip
geom	=	due to the geometry
s	=	in the steady state condition

I. Introduction

THE civil aviation industry is facing wide-ranging changes to reduce its overall impact on the environment, in particular these changes are focused on reducing the carbon footprint of air transport which currently accounts for 2% of emissions globally [1]. Recent initiatives such as the ICAO's CORSIA scheme [2] aim to put a cost on emissions, incentivizing the aviation industry to find more radical solutions to improve the efficiency of aircraft. One way in which this goal can be achieved is by reducing the overall aerodynamic drag, of which a primary contributing factor is lift-induced drag which can be reduced by increasing the wing aspect ratio. There are many next-generation concepts aiming to dramatically increase this value. However, such an increase leads to higher bending moments and extra structural weight. Perhaps more importantly, an increase in span changes the operational costs and requirements of an aircraft, with airport fees calculated according to the span and current infrastructure at many airports only capable of servicing aircraft up to a specific span.

Folding Wingtip (FWT) devices, in which the span of the aircraft can be shortened by folding the wingtips up on the ground, have gained much interest with many next generation aircraft aiming to include them. This type of device is not new, with military aircraft using the concept to save space on aircraft carriers as early as the first world war. The most notable recent application is the Boeing 777X which first flew in 2020, allowing the aircraft to fit into the same 65m gate as its predecessor whilst also being able to increase its wing-span in flight by 7m. Whilst this device can only be operated on the ground, the inclusion of such a mechanism poses the question as to whether it can be utilized in-flight for both aerodynamic and structural benefits, particularly as the large moment arm of a wingtip means it has a significant influence on the bending moment distribution along the wing.

Recent research has considered using FWTs as a load alleviation device and one particular concept that has gathered traction is that of the Flared Folding Wingtip (FFWT) [3–10]. As illustrated in Fig. 1 this device consists of a FWT in which the hinge line has been rotated to move the intersection with the leading edge outboard so that the hinge line is no longer parallel with the oncoming flow, with the magnitude of this rotation being defined as the flare angle (Λ). In this configuration an increase in the fold angle (θ) produces a decrease in its local Angle of Attack (AoA), and vice versa in the other direction. Therefore, when a FFWT is free to rotate, the fold angle tends to an equilibrium position, defined as the coast angle, about which the system is statically stable. Using the assumption of small fold angles it has previously been shown that this relationship can be described as [5]

$$\Delta \alpha = -\arctan\left(\sin \Lambda \tan \theta\right) \tag{1}$$

Initial numerical results have showcased the potential of such a system on a representative civil airliner for gust alleviation [6] with experimental results verifying this potential [5, 10]. Following on from these initial results, other studies have aimed to quantify the aeroelastic response and stability behaviour of FFWTs across the entire flight envelope.

One key area of research is the roll performance of an aircraft, as for a fixed configuration the maximum achievable roll rate is approximately proportional to the inverse of the span cubed, due to the increase in aerodynamic roll damping (see section II). Further to this, increasing the span increases the moment of inertia of the aircraft, reducing the rate of acceleration for a given aileron torque. Hence, for a conventional aircraft configuration, a push towards larger spans would require a significant increase in aileron sizing to maintain the same roll behaviour, which may be structurally unfeasible or lead to an earlier onset of aeroelastic phenomena such as aileron reversal. Therefore, future aircraft designs with increased spans may need to incorporate aerodynamic roll damping alleviation techniques to ensure adequate controllability. With major airworthiness authorities defining a minimum time for a civil aeroplane to complete a defined roll as
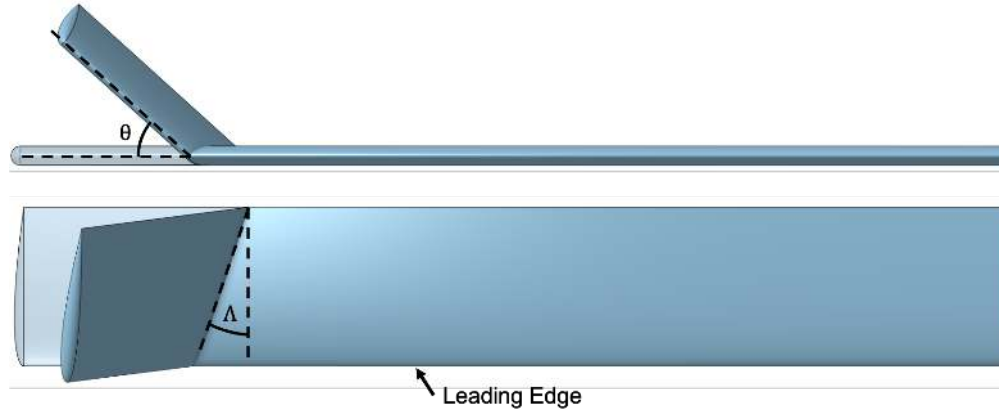
Fig. 1   Representation of a flared folding wingtip device, with a flare angle (Λ) of 20 degrees, at 0 and 45 degrees fold angle (θ)

FAA Regs Sec. 23.157: Rate of roll [11] -   Takeoff. It must be possible, using a favorable combination of controls, to roll the airplane from a steady 30-degree banked turn through an angle of 60 degrees, so as to reverse the direction of the turn within:

1) For an airplane of 6,000 pounds or less maximum weight, 5 seconds from initiation of roll; and
2) For an airplane of over 6,000 pounds maximum weight, $\frac{(W+500)}{1,300}$ seconds, but not more than 10 seconds, where W is the weight in pounds

EASA AMC 25.253(a)(4) Lateral Control: Roll Capability [12] -   Establish a steady 20 degrees banked turn at a speed close to V_{DF}/M_{DF} (the demonstrated flight diving speed) limited to the extent necessary to accomplish the following manoeuvre and recovery without exceeding V_{DF}/M_{DF}. Using lateral control alone, it should be demonstrated that the aeroplane can be rolled to 20° bank angle in the other direction in not more than 8 seconds. The demonstration should be made in the most adverse direction. The manoeuvre may be unchecked.

Regarding FFWTs, results developed using a simple model [8] highlighted that FFWTs may produce significant aerodynamic roll damping alleviation, with maximum roll rates shown to be greater than that of a wing with the additional span removed [8]. This work was further developed in later studies [9] in which the aeroelastic effects of FFWTs were coupled with an aircraft's flight dynamics equations. It was found that an aircraft incorporating FFWTs would have similar handling capabilities to one without the additional span. These studies indicate the possibility that this type of device could be used to extend the wing span of existing designs without either large changes to control surface area or the aircraft's operational requirements. These studies have however been limited to low fidelity numerical modeling and have also only considered the linear behaviour of an aircraft about a roll angle of zero degrees. Therefore, they have not considered how the orientation of the gravitational vector may also affect the performance.

A. Objective of Paper

The aim of this paper was to investigate the effect of FFWTs on the roll performance of rectangular, unswept, untapered wings. The first section describes the development of a wind tunnel model that is used to assess the effects of FFWTs, which are beneficial for gust load alleviation, on the roll authority of a wing for a given span. In the second section, a mathematical model is developed to compare predictions with the experimental data for both steady and transient responses. The design space is then further explored to demonstrate how FFWTs can be utilised to significantly increase an aircraft's effective span, without a reduction in roll authority.

II. Basic Anatomy of a Roll Maneuver

Despite its apparent simplicity, the dynamics of rolling an aircraft are quite complex. When a pilot inputs a roll command, the resulting aileron deflections produce an asymmetric span-wise lift distribution. This asymmetry produces

a torque leading to a change in the angular rate of the aircraft. For simple analysis this torque can be considered as

$$\tau_a = \frac{1}{2}\rho V^2 c C_\beta \beta \tag{2}$$

where C_β is the control surface torque coefficient and β is the aileron deflection. As the roll rate increases there is a further change to the lift distribution as the rolling motion induces a vertical velocity component (w) along the span of the wing, changing the local AoA such that

$$\alpha_i = \arctan(\frac{w}{V}) \approx \frac{w}{V} = \frac{-yp}{V} \tag{3}$$

where p is the roll rate of the aircraft and y is the distance from the centre of rotation. This change in the AoA produces a negative aerodynamic force on the side going up and a positive force on the side going down, producing a torque that opposes the rolling motion called aerodynamic roll damping ($\tau_r(p)$). For a simple wing geometry, and assuming the local lift coefficient does not vary as a function of the span, the aerodynamic roll damping can be approximated as

$$\tau_r(p) = 2 \int_0^{s/2} \tilde{L} y \, dy = 2 \int_0^{s/2} (\frac{1}{2}\rho V^2 c \frac{dC_l}{d\alpha}\alpha_i) y \, dy = -\frac{1}{24}p\rho V c \frac{dC_l}{d\alpha} s^3 \tag{4}$$

where $\tilde{L}$ is the local lift per unit span and C_l is the local lift coefficient. By including the moment of inertia (I_{xx}), the equation of motion for a fixed wing aircraft completing a simple roll maneuver can be approximated as

$$\tau_a - \tau_r(p) = I_{xx}\dot{p} \tag{5}$$

This is a simple first order differential equation, and when considering the initial condition of the wing being at rest, the exact solution is

$$p(t) = \frac{\tau_a}{\tau_r}\left(1 - \exp\left(\frac{-\tau_r}{I_{xx}}t\right)\right) \tag{6}$$

From these equations we can see that as the roll rate increases so does the aerodynamic roll damping until it is equal and opposite in magnitude to the aileron torque, at which point the aircraft will maintain a steady roll rate (p_s), with a value equal to

$$p_s = \frac{\tau_a}{\tau_r} = \frac{12VC_\beta\beta}{C_L s^3} \tag{7}$$

This means a typical roll maneuver can be split into two regions that are both important when assessing the overall roll performance of an aircraft. Firstly, there is the *Roll Acceleration* region in which an aircraft accelerates from a roll rate of zero to the steady roll rate. The size of this region, in terms of time, is dominated by the time constant of the system, which from Eqn. 6 can be seen to be proportional to the inverse of the aerodynamic roll damping. Secondly, there is the *steady roll rate* region in which an aircraft maintains a steady roll rate that is also proportional to the inverse of the aerodynamic roll damping. As such the experimental and numerical models used within this paper have been developed to capture both of these regions to give a boarder picture on the effects of using FFWTs on the roll performance of an aircraft.

III. Experimental Rig

A. Design

The primary aim of this investigation was to assess the aerodynamic roll damping alleviation properties of a wing incorporating FFWTs and the effect this has on the steady and transient roll behavior. A rolling rig comprising a symmetric rectangular wing was designed that could achieve and maintain, from a standing start, a steady roll rate within the working section of the 7ft by 5ft low-speed closed-return wind tunnel at the University of Bristol.

As shown in Fig 2, a drive shaft was located centrally in the working section, along with an electromechanical brake to both hold and release the shaft. The center of a model wing could be attached to the shaft, allowing it to rotate freely about its roll axis. This wing had a maximum span of 1m, a constant chord of 67mm and the constant sectional profile of NACA0015. Its design included a central connector and an aluminium spar over which three 100mm inner wing sections could be attached on each side. The thickness of the aluminium spar meant that for the purposes for this experiment the inner wing could be considered a rigid body.

The tip of the wing could be easily replaced, allowing multiple wingtip configurations to be tested. During this investigation four wingtip configurations were used:
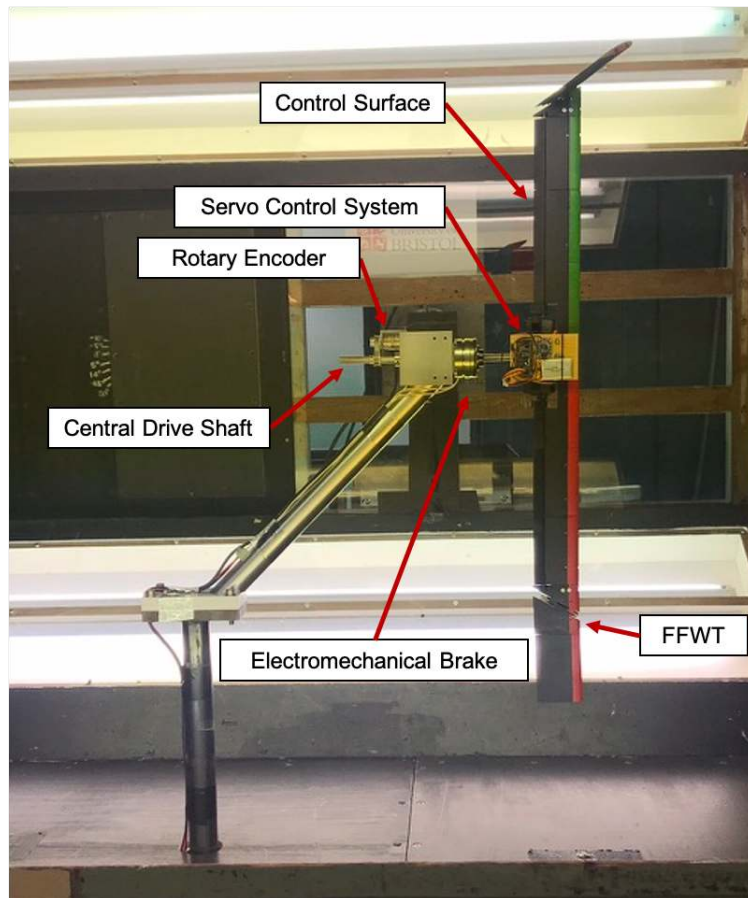
Fig. 2   Wind tunnel model to assess the rolling performance of Flared Folding Wing Tips
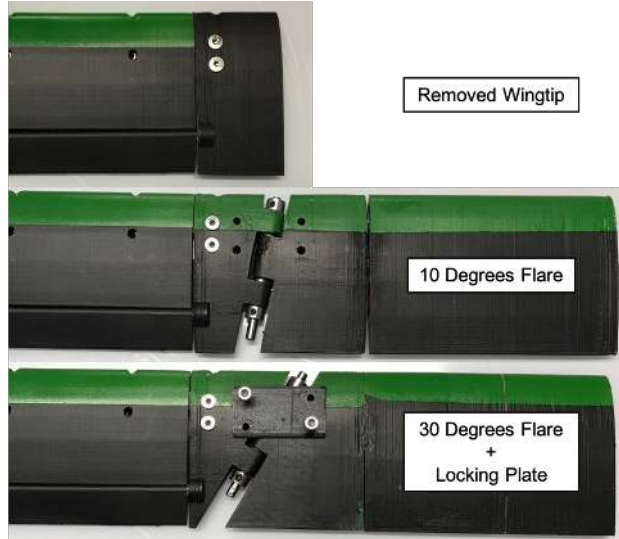
Fig. 3   An overview of the four wingtip configurations used during the investigation

Table 1   Reference parameters for the four wingtip configurations

Configuration	Span [mm]	Flare Angle [deg]
Removed	728	-
Fixed	1000	-
Free 10	1000	10
Free 30	1000	30

- a baseline wing with a total semi-span of 364mm
- two FFWTs with flare angles of 10 and 30 degrees,with a total semi-span of 500 mm. In these designs the hinge line crossed the semi-chord line at a semi-span of 364mm
- a fixed configuration in which the fold angle of the FFWTs is fixed at 0 degrees by replacing a locking plate across the hinge

An overview of these configurations can be seen in Fig. 3 and a summary of their parameters can be seen in Table 1.

The roll rate of the model could be controlled by deflecting two control surfaces which spanned the entire length of the inner section on both sides of the model. These were actuated in an opposing manner by two servo motors which were attached to the central section. A battery and an Adafruit Feather micro controller[*] were also attached to the central section to both power and control the servo motors wirelessly.

B. Instrumentation

The wind tunnel model was equipped with an RLS RE22[†] rotary encoder located on the central shaft to measure the roll angle of the model. The encoder was connected to a National Instruments PXIe-6363[‡] card hosted in a National Instruments PXIe-1082 chassis, with the Matlab Data Acquisition API being utilised to collect the data.
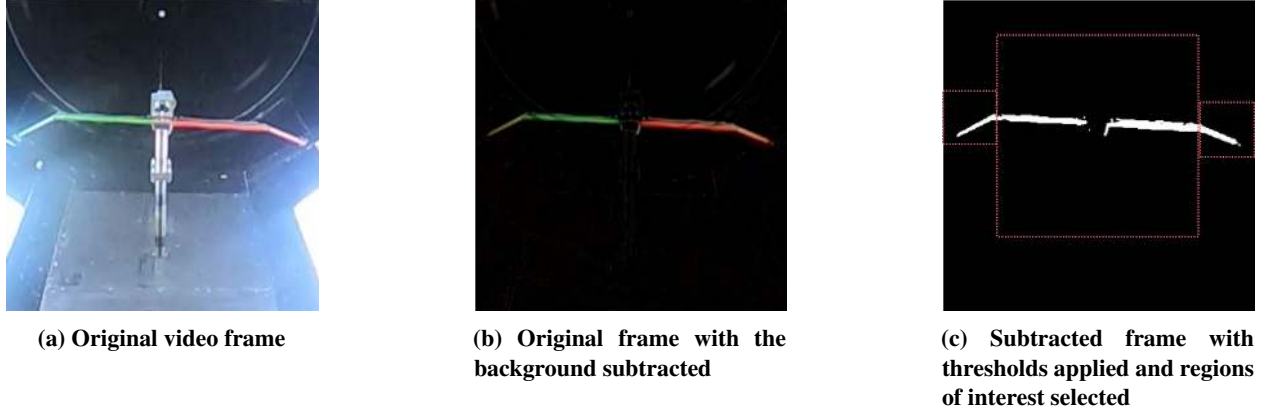
Additionally, the fold angle of the wingtips was recorded at 120 Hz using a GoPro Hero 8[§] placed upstream of the model. As shown in Fig. 2 and Fig. 4a, the leading edge of the left and right side of the model were painted green and red respectively. By removing a background image from each frame (Fig. 4b) and applying a threshold for green and red pixels, a binary image could be created showing the location of the leading edge (Fig. 4c). From this image, a cropped section about the centre of the model could be selected to only show pixels which are part of the inner wing,

---

[*]URL: https://www.adafruit.com/feather, date accessed: 18/11/2020

[†]URL:https://www.rls.si/eng/re22-rotary-magnetic-shaft-encoder, date accessed: 18/11/2020

[‡]URL:https://www.ni.com/en-gb/shop/pxi.html, date accessed: 18/11/2020

[§]URL:https://gopro.com/en/gb/, date accessed: 18/11/2020

(a) Original video frame

(b) Original frame with the background subtracted

(c) Subtracted frame with thresholds applied and regions of interest selected

Fig. 4 **An overview of the computer vision algorithm used to measure the roll and fold angles of the wind tunnel model**

Table 2 **Test Matrix for the transient release of the rolling model**

Parameter	Value
Model Configuration	Removed, Fixed, Free10, Free30
Wind Tunnel velocity [m s^{-1}]	15,20,25,30
Aileron Deflection [deg]	7,14,21

allowing the roll angle to be calculated by fitting a line through these pixels. Two further regions of interest could then be selected from the binary image that represent the possible locations of the FFWTs, enabling the fold angles to be calculated in a similar fashion.

C. Methodology

The 7ft by 5ft low-speed closed-return wind tunnel at the University of Bristol was used to test each wing tip configuration at four airflow velocities[¶] and three aileron angles, as summarised in the test-matrix shown in Table 2. At each test point the model was first locked using the electromechanical brake in the horizontal position, the aileron angle was set, then the brake was released and the rig allowed to spin freely for 10 seconds. The process was repeated three times at each test point. GoPro data, used to calculate the fold angles, was recorded for one run at each test point.

IV. Mathematical Modelling

A. Structural Model

A simplified three Degrees of Freedom (DoF) model, seen in Fig. 5, of a rectilinear wing of span s and chord c, was developed to compare with the experimental results as well as to further explore the design space. This mathematical model is geometrically non-linear and includes the effect of gravity; it consists of an inner wing and two FFWTs that are represented as point masses with a specific mass and moment of inertia. The percentage of the span taken up by the FFWTs is denoted σ and the generalised coordinates of this system are the roll angle ϕ (about the centre of the model) and the fold angle θ_1, θ_2 of each FFWT

$$\mathbf{q} = \begin{bmatrix} \phi \\ \theta_1 \\ \theta_2 \end{bmatrix} \tag{8}$$

All motion is assumed to occur in a 2D-plane, hence the moment arm of each FFWT with respect to the hinge (l_f) is corrected by the cosine of the flare angle to account for the angle between the spanwise direction and the direction

---

[¶]Selected velocities were between 15 and 30 m s^{-1}, giving an approximate Reynolds number range of 70,000 to 140,000
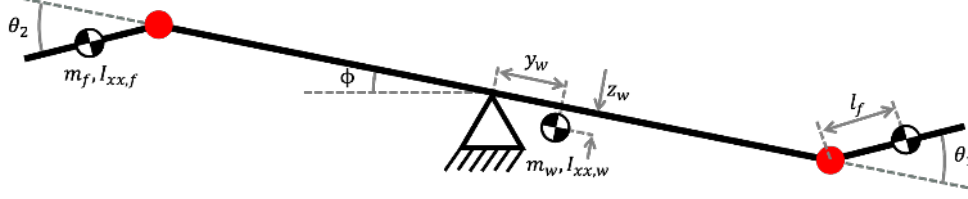
7

Fig. 5 Diagrammatic representation of the three degree of freedom mathematical model, as viewed from downstream of the model

Table 3 Parameters used to calculate the three lift distributions

Distribution	Span [mm]	Root AoA [deg]	Roll Rate [deg s^{-1}]	Wingtip Twist [deg]
Roll60	1000	0	60	0
Roll60-Removed	768	0	60	0
Wingtip-Twist	1000	0	0	2

perpendicular to the hinge. Additionally, the experimental model was not balanced about the centre of rotation due to differences in material densities between 3D printed parts and the addition of the control mechanism. Hence, as shown in Fig. 5 the Centre of Mass (CoM) of the main wing (m_w) is offset from the centre of rotation by y_w and z_w in the y and z direction respectively. The equations of motion of this system were found using the Euler-Lagrange method utilising the python package sympy [13], and were of the form

$$M\left(\mathbf{q},\dot{\mathbf{q}}\right)\ddot{\mathbf{q}} - f\left(\mathbf{q},\dot{\mathbf{q}}\right) = 0 \tag{9}$$

where M is the mass matrix and f is a matrix of additional forces.

B. Aerodynamic Model

The aerodynamic forces acting on the wing were modeled using modified strip theory at a discrete number of panels, with the main wing being split into 20 uniform panels and each FWT being split into 10. At each panel the local AoA is calculated as

$$\alpha(y) = \alpha_{\text{geom}} + \frac{w(p,y)}{V} \tag{10}$$

where α_{geom} represents the geometric AoA. For the inner wing α_{geom} is assumed zero, and for each FFWT it is modelled using Eqn. 1.

To account for 3D effects, the local lift coefficient at each panel was interpolated from a set of lift distributions that were pre-calculated using lifting line theory. The purpose of this paper is not to accurately predict this lift distribution, as it is likely to vary as a function of not only velocity and root AoA but also the fold angle of each wingtip. Therefore, a set of lift distributions were calculated to best represent the mean case as well as to indicate the sensitivity of the results to the underlying distribution.

In total three distributions were calculated utilising the python package aerosandbox [14], with a comparison between them being shown in Table 3 and Fig. 6. Two distributions were created for a symmetric rectilinear wing of two spans (to represent the fixed and removed case in Table 1) in a single operating condition; a root AoA of 0 degrees and a roll rate of 60 deg s^{-1}. The third distribution aimed to mimic the distribution seen in the steady level condition by applying a twist of 2 degrees to panels outboard of the hinge line, with the model at a root AoA of 0 deg.

Aerodynamic forces were converted into generalised coordinates using the principle of equal wrench's [15], which emanates from D'Alembert's principle.

C. Numerical Integration

The final form of the equations of motion were formulated as

$$M\left(\mathbf{q},\dot{\mathbf{q}}\right)\ddot{\mathbf{q}} - f\left(\mathbf{q},\dot{\mathbf{q}}\right) = g\left(\mathbf{q},\dot{\mathbf{q}}\right) \tag{11}$$

8
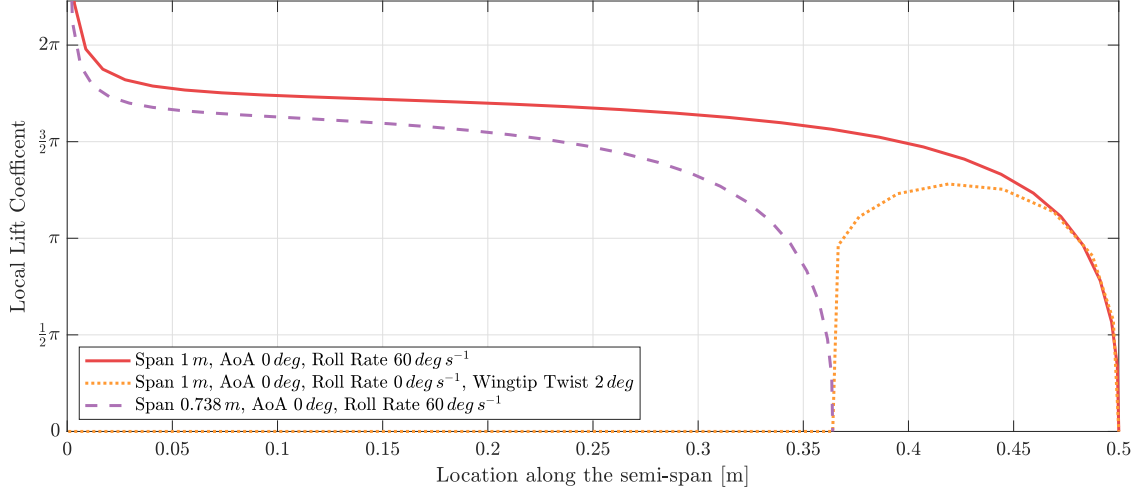
Fig. 6   A comparison of the three lift distributions used in the simulated results

Table 4   Mass parameters used in the simulations

Configuration	Removed	Fixed	Free10, Free30
Wing Mass [g]	759	884	773
Wing Inertia [kg m^2]	1.77×10^{-2}	3.98×10^{-2}	1.95×10^{-2}
y_w [mm]	2.01	0.57	1.98
z_w [mm]	2.76	2.38	2.73
FWT Mass [g]	0	0	50
Wing Inertia [kg m^2]	0	0	8.7×10^{-5}
FWT Moment Arm [mm]	0	0	76.6

where $g\left(\mathbf{q}, \dot{\mathbf{q}}\right)$ represents the external forces, including aerodynamic forces. The model was solved for the same configuration and test points as those conducted in the wind tunnel experiments. The specific parameters for each configuration can be seen in Table 4 and an overview of the test matrix can be seen in Table 2.

Firstly, at each test point the steady coast angle of each FFWT was calculated by finding the roots of Eq. 11 when $\ddot{\mathbf{q}} = \dot{\mathbf{q}} = 0$. These were then used as the initial conditions for numerical integration. To simulate the aileron torque an additional external force was applied to the model of the form

$$g_\tau \left(\mathbf{q}, \dot{\mathbf{q}}\right) = \begin{bmatrix} \tau(t, V) \\ 0 \\ 0 \end{bmatrix}, \quad \tau(t, V) = \begin{cases} \frac{t}{\tau_0} \left(\tau_1 V^2 + \tau_2\right) & t < \tau_0 \\ \tau_1 V^2 + \tau_2 & t \geq \tau_0 \end{cases} \tag{12}$$

where τ_0 controls the jerk of the torque profile - which is the derivative of the acceleration, and τ_1 and τ_2 are constants that were tuned for each aileron angle to match the experimental results of the removed case. A diagrammatic representation of this external force can be seen in Fig. 7. The python package scipy was used to integrate the model until three complete revolutions were completed.

V. Results

Prior to the release of the electromechanical brake, the fold angle of each wingtip achieved a stationary position, corresponding to the coast angle at which the aerodynamic and gravitational moments about the hinge balanced. A comparison of the experimental and simulated coast angles for the fixed brake case across all velocities is shown in Fig. 8. As the air speed increases, a smaller local AoA is required on a wingtip to produce the same aerodynamic force, reducing the coast angle. In the limit of the velocity tending to infinity, the local AoA must tend to zero. Therefore, for a
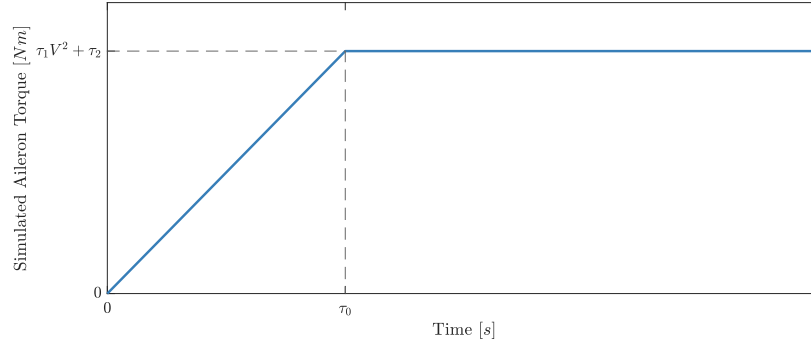
**Fig. 7   A diagrammatic representation of the external torque applied to the numerical model**
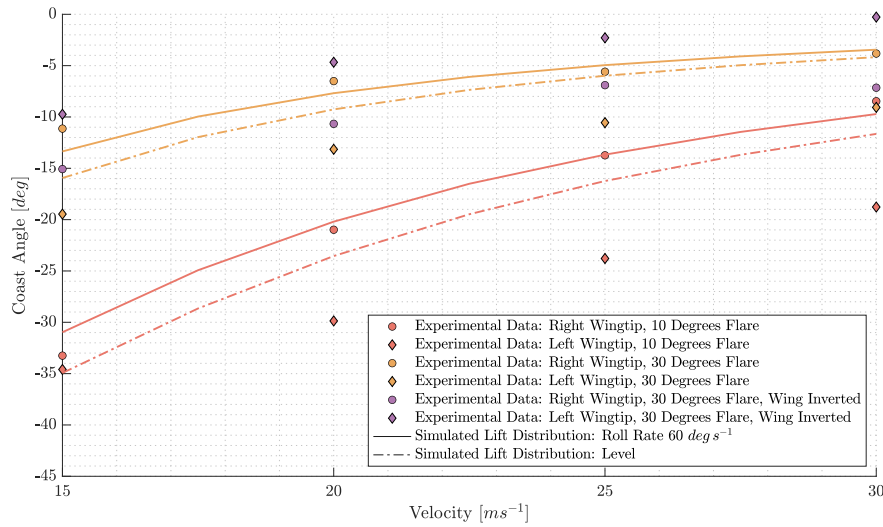
Fig. 8   The coast angle of each wingtip with flow speed, for each model configuration

straight symmetric FFWT the coast angle will also tend to zero. The numerical results follow a similar qualitative trend to that of the experimental data, with the choice of lift distribution having a second order effect.

However, Fig. 8 indicates there is a disparity between the coast angles of the left and right wingtip. Furthermore, the inverted case in Fig. 8 (at which the model was held at a roll angle of 180 degrees) shows that the fold angle of the wingtip on the left hand side of the tunnel was always lower. The cause of these variations is assumed to be either a miss-alignment of the model - as any side-slip would increase the relative flare angle on one side of the model and decrease it on the other; or some flow non-uniformity either inherent in the flow or caused by the presence of the strut. As lower flare angles are more sensitive (a larger change in fold angle is required to get the same change in aerodynamic force) you would expect the variation to be larger for the 10 degrees configuration, as is the case in Fig. 8.

Following the release of the model, example experimental and numerical roll rate and roll acceleration time traces for the fixed, removed and free-30 configurations at a velocity of $25\,\mathrm{m\,s^{-1}}$ and an aileron angle of 14 degrees can be seen in Fig. 9. In this figure two distinct regions can be identified, the *Roll Acceleration* region in which the roll rate grows from zero to around the steady roll rate, and the *Steady Roll Rate* region in which the roll rate oscillates about a constant value. The results in this section are displayed according to these two regions, initially concentrating on the *Steady Roll Rate* region, and then on the *Roll Acceleration* region. These initial results show that the average steady roll rate for the removed case is much greater than that of the fixed case, and that the 30 degree free case achieves around 80% of the removed case value. The initial accelerations of the removed and free cases, following release of the brake, are around twice the fixed case values.

10
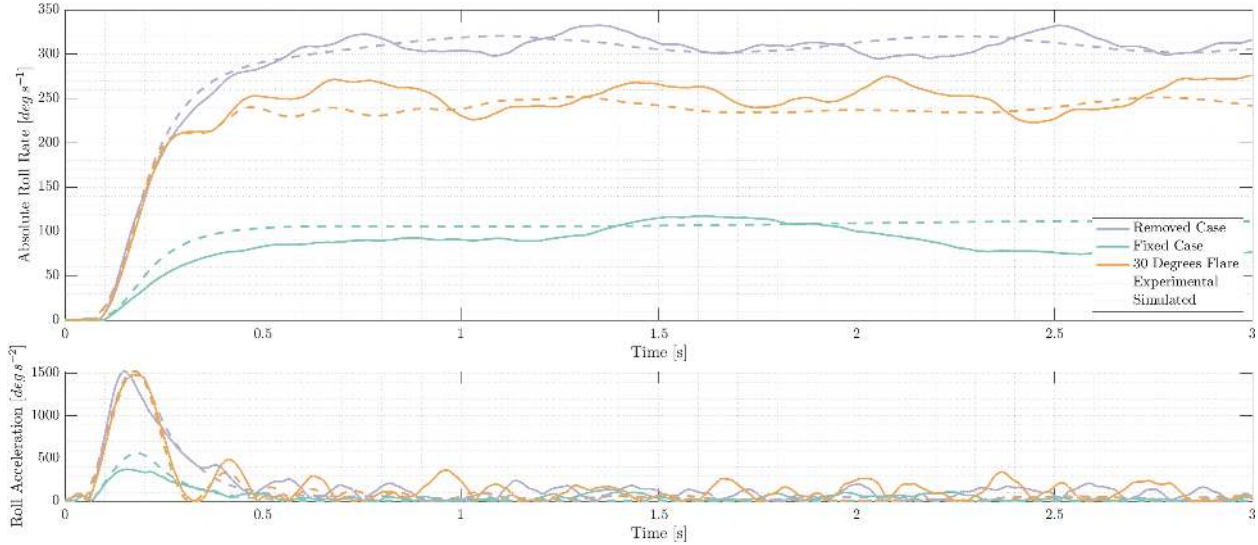
Fig. 9 Example experimental and numerical time traces for the removed, fixed, and free30 configuration at 25 m s^{-1} and aileron angle of 14 degrees

A. Steady Roll Rate

1. Mean Response

To calculate the mean steady roll rate at each test condition, the mean roll rate was calculated for each repeated test across the last two complete rotations of the model, ensuring values are not biased towards towards particular roll angles. The average value across the three repeat tests was then calculated, with the results shown in Fig. 10, along with the results normalised by the simulated removed case at each velocity.

Figure 10 shows that the mean steady roll rate for the fixed case is much less, around 70%, compared to the removed case. Utilising FFWTs significantly increased the mean steady roll rate when compared to the fixed wing of the same total span, but did not achieve that of the removed case, with only a 50-75% recovery of the mean roll rate achieved. The magnitude of this recovery was larger for larger flare angles and furthermore, the reduction is dependent on the aileron angle, with larger angles reducing the effectiveness of the FFWTs. These conclusions can be draw from both data sets, with good correlation being shown between the simulated and experimental results.

The variations in steady roll rate and hence the aerodynamic roll damping for the free cases are driven by changes to the fold angle of the FFWTs. Fig. 11 shows the average fold angle across the last two complete rotations for each wingtip at each test point. As the wing profile is symmetric, the mean fold angles of the left and right wingtip should be identical, albeit inverted (a positive fold angle of the left wingtip at zero degrees roll is the same as a negative fold angle on the right wing tip at 180 degrees roll).

The fold angle of a FFWT is defined by a balance of three forces acting about the hinge. These forces are the aerodynamic, inertial and gravitational forces acting on the wingtip.

Considering only the aerodynamic forces, the relationship between the fold angle and the local AoA, described in Eq. 1, tends to move the wingtip to the *zero moment angle*, at which the net aerodynamic moments acting about the hinge are zero. For a stationary straight symmetric wing this case corresponds to the zero fold angle, as the AoA across the entire wingtip will be zero. However, for a given non-zero roll rate the induced AoA due to the motion of the wing, described by Eq. 3, shifts the zero-moment-angle to a non-zero fold angle which 'lags' the motion of the inner wing, as shown in Fig. 11. At this angle the contribution of the FFWTs to aerodynamic roll damping is reduced when compared to that of the fixed wing, as illustrated in Fig. 12. As shown in Eqn. 7 reducing aerodynamic roll damping increases the mean steady roll rate, and hence this effect is the primary mechanism increasing the steady roll rates in Fig. 10.

Two major assumptions were made during this analysis. Firstly, the underlying lift distribution has been assumed to be invariant of the fold angles. At low fold angles this assumption may be acceptable, but at larger fold angles such as seen in the 10 degrees hinge case, there may be significant changes in this lift distribution which may account for the larger discrepancies seen in Fig. 11. Secondly, when looking at region 1b in Fig. 12, the lift distribution about the

11
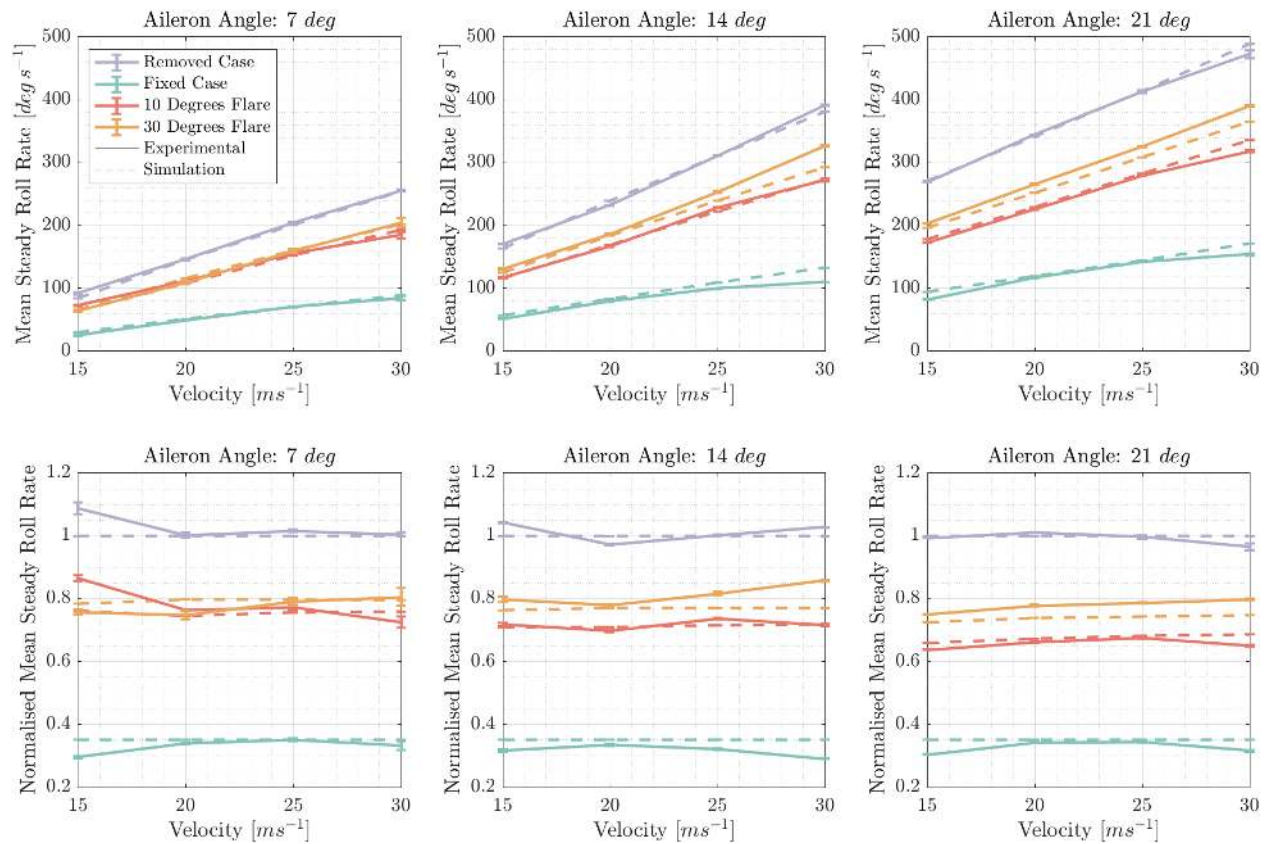
Fig. 10   Mean steady roll rates at each aileron angle and velocity for each model configuration. In the bottom row values have been normalised by that of the simulated removed case at each velocity
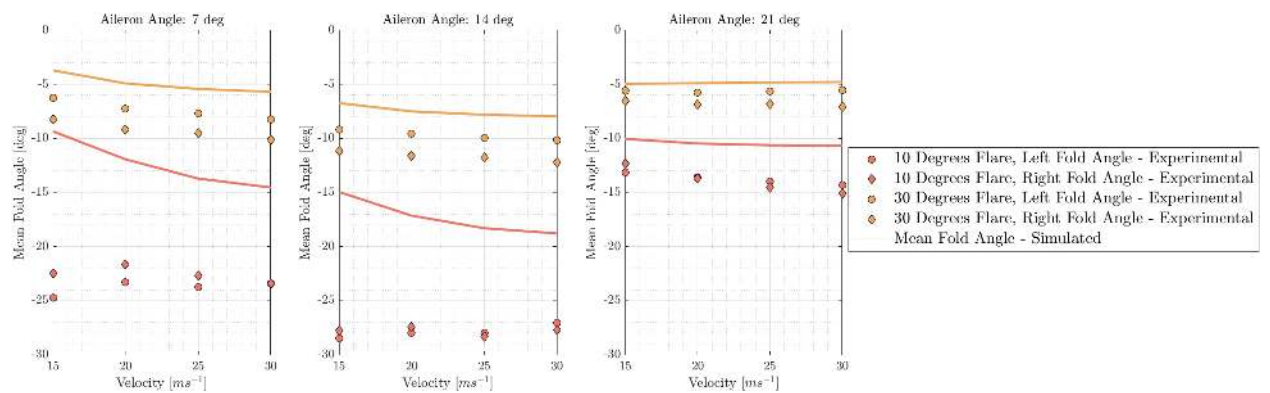
Fig. 11   The mean fold angle of each wingtip at each aileron angle and velocity for each model configuration
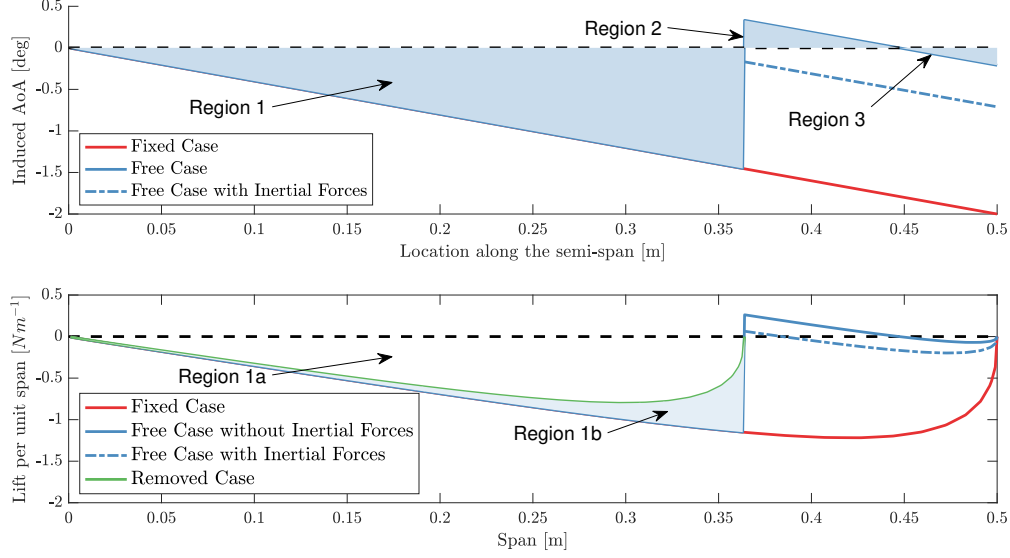
Fig. 12 **A diagrammatic representation of the aerodynamic and inertial forces acting on the fixed, free and removed case due to a rolling motion of $60 \deg s^{-1}$**

hinge is unrealistic as there would be a drop off in the magnitude of the lift either side of the step change in local AoA, potentially further increasing the roll damping alleviation properties of FFWTs.

As the induced AoA due to the rolling motion varies along the wingtip, the contribution of the wing to roll damping can be split into the three regions shown in Fig. 12. Region 1 corresponds to the roll damping produced by the inner wing. Region 2 corresponds to the inner section of the wingtip which produces a force that aids the rolling motion. Region 3 corresponds to the outer section of the wingtip and positively contributes to roll damping. At the fold angle at which a wingtip is in equilibrium, the moments about the hinge from regions 2 and 3 must cancel, and as region 2 is closer to the hinge it must produce a larger force. Hence, when only aerodynamic forces are considered and recalling only shear forces are transmitted through a hinge, a FFWT must have a net negative contribution to aerodynamic roll damping. To emphasize this point, if the inner wing was replaced with a rod that had zero contribution to roll damping, the FFWTs would still drive the motion.

It should also be noted that the induced AoA in regions 2 and 3 is just an offset of that of the fixed case. Hence, when only considering aerodynamic forces at small fold angles, the roll damping alleviation of a FFWT will be independent of the flare angle, as different flare angles will tend to a different zero-moment-angles, producing the same induced AoA distribution.

Regarding only inertial forces, when a wingtip is stationary these forces are zero. However, at a constant roll rate the centrifugal forces acting in the reference frame of the wingtip tend to move the wingtip towards an equilibrium position pointing radially from the centre of rotation, which in the case of a straight wing corresponds to the zero fold angle. The magnitude of this force on the right wingtip can be approximated as

$$\tau_c = \left(\frac{s(1-\sigma)}{2} p^2 \right) \times \left(l_f \, m_f \, \sin \theta_1 \right) \tag{13}$$

where the first term represents the centrifugal acceleration.

In the case of a straight symmetric wing at a constant roll rate, the zero-moment-angle is pulled back so that the wingtip lags the motion of the inner wing. Hence, the centrifugal forces, which act towards the zero fold angle, pull the wingtip away from its 'ideal' location, reducing the roll damping alleviation of the FFWT, as shown in Fig. 12. When the flare angle is decreased the zero-moment-angle increases, and as the centrifugal forces are proportional to the sine of the fold angle, smaller flare angles induce larger inertial forces, reducing the roll damping alleviation of FFWTs. This conclusion partially explains the difference between the 10 and 30 degree hinge case in Fig. 10.

Furthermore, consider the magnitude of the aerodynamic and centrifugal forces acting on a wingtip at varying roll rates. The aerodynamic forces are proportional to the local AoA and therefore, as shown in Eqn. 3, are linearly proportional to the roll rate whereas Eqn. 13 shows that the centrifugal forces are proportional to the roll rate squared.
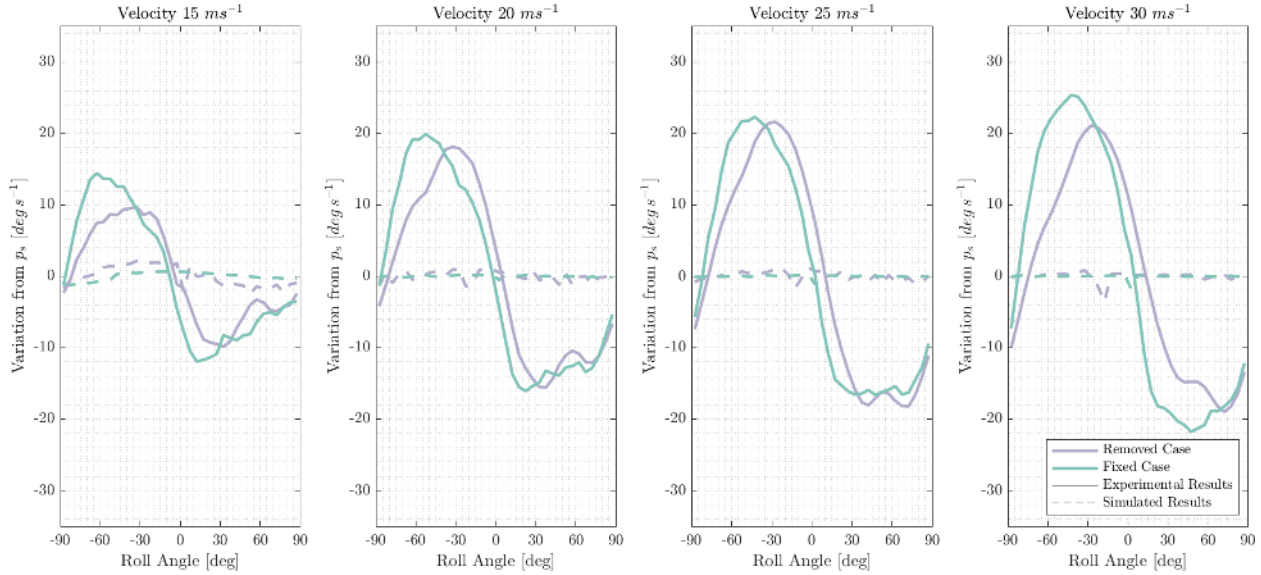
Fig. 13 Variation from the steady roll rate with roll, for each configuration at multiple velocities and an aileron angle of 7 degrees

Consider steadily increasing the roll rate of a wing from zero. At low roll rates aerodynamic forces will dominate and the coast angle of a FFWT will increase to reduce the local AoA. As the roll rate increases further, centrifugal forces will start to dominate pulling the wingtip back towards the zero fold angle. This effect may explain why the fold angle increases between an aileron angle of 7 and 14 degrees in Fig. 11 but then reduces as the aileron angle increases to 21 degrees.

However, in general, the inertial forces need not always reduce the roll damping alleviation of FFWTs. If the zero-moment-angle instead leads the motion of the wing, which can be achieved by adding camber to the wingtip, the inertial forces will increase the local AoA, increasing aerodynamic roll damping alleviation.

2. Cyclic Response

It can be clearly seen in Fig. 9 that the steady roll rate is not constant with time in the *steady roll rate* region, and instead oscillates about a mean value. For a balanced wing, in the fixed and removed case, no oscillation should be seen in this region, however due to the CoM being offset, changes in the roll rate at a frequency matching the rotational frequency of the rig were expected. These oscillations should however be symmetric about positive and negative roll angles.

By taking the modulo of the roll angle by 180 (to cancel variations due to the offset mass), splitting these values into 36 segments with a width of 5 degrees, and averaging all roll rates that occur in each window, these oscillations can be visualised with respect to the roll angle, as shown in Fig. 13. The roll rate in the simulated fixed and removed case in Fig. 13 is independent of the roll angle as expected. However, variations are present in the experimental data, occurring twice per revolution. The cause of these variations is still under investigation, but as these oscillations are seen in the cases with no folding wingtips it is assumed not to be a model alignment issue but instead be due to non-uniformities in the flow field.

By taking the mean line of the variations seen in Fig. 13 as the baseline and calculating the delta between this baseline and the other configurations, a more representative comparison can be made between the numerical and experimental results. Figs. 14 and 15 show that with the inclusion of the FFWTs additional variations (above that of the baseline) are seen in the roll rate of the model with respect to the roll angle. Depending on the test point the magnitude of these variations varies from ±5% to ±25% of the steady roll rate, with a significant proportion of these variations occurring between ±60 deg roll (the typical operating range of an aircraft). As with the mean response these variations are due to changes in the fold angle of the wingtips and in this case are primarily driven by the gravitational forces acting on the wingtips.

Considering only gravitational forces, a wingtip acts as a pendulum with a stable equilibrium position pointing
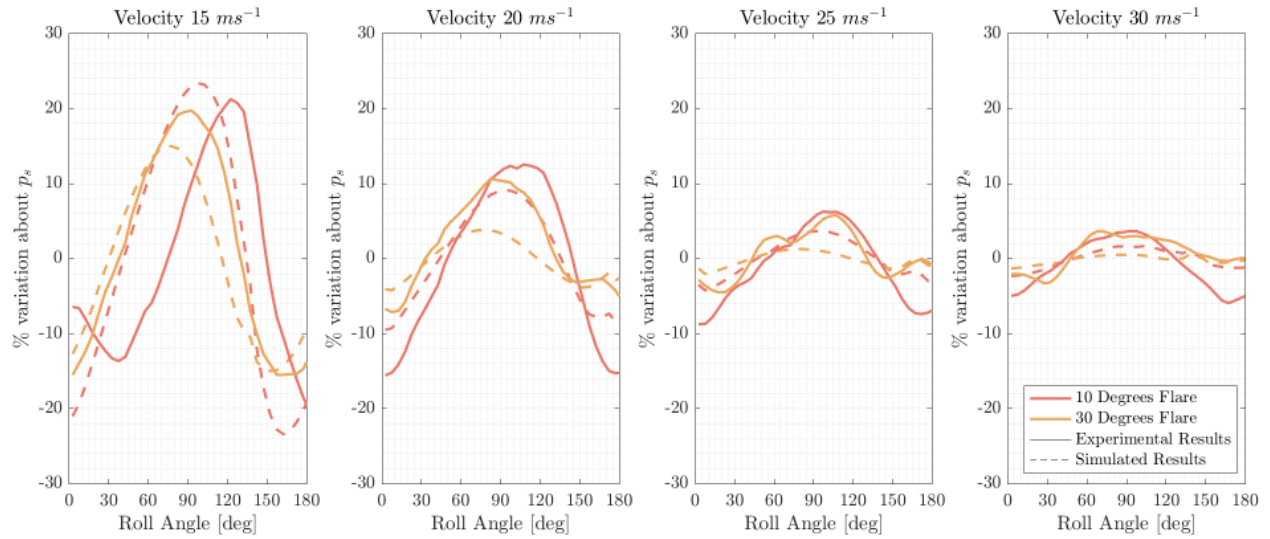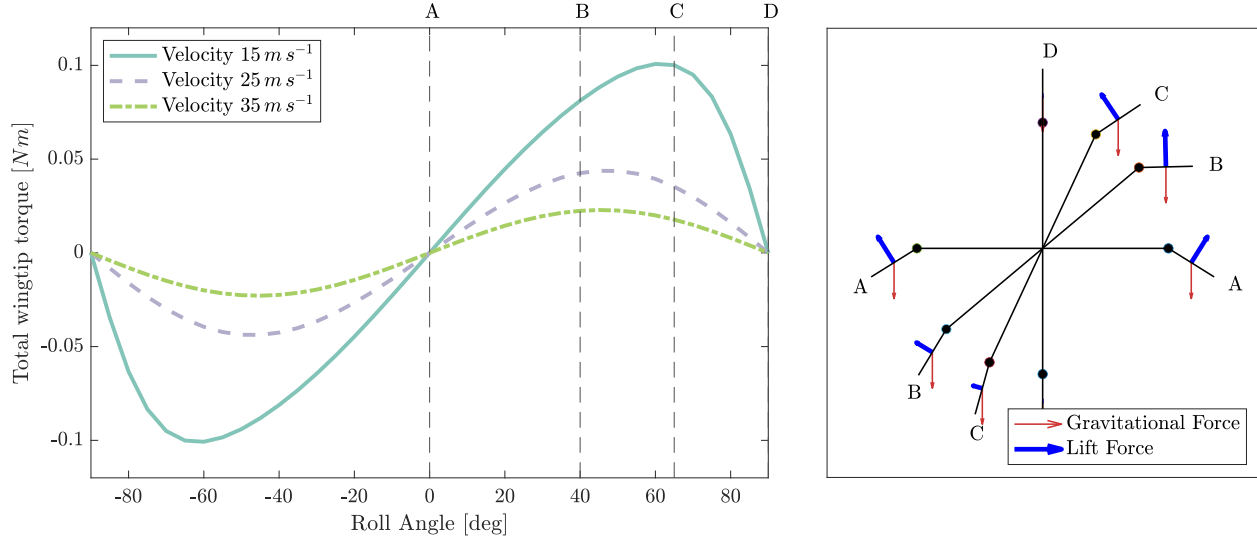
Fig. 14 **Variation with roll of the roll rate as a percentage of the steady roll rate, for each configuration at multiple velocities and an aileron angle of 14 degrees**
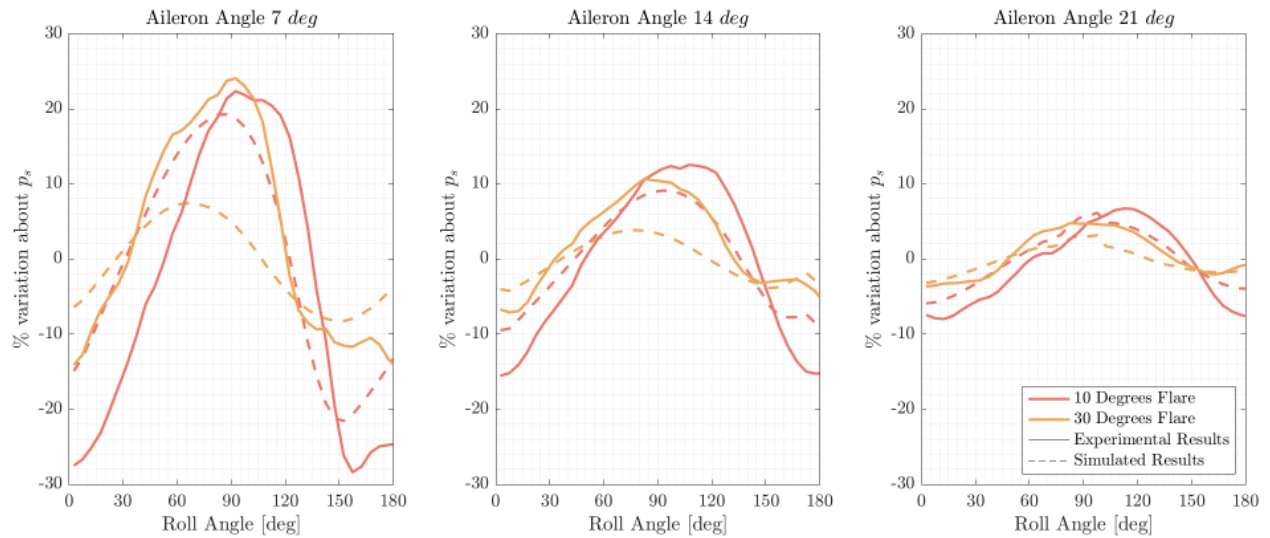
Fig. 15 **Variation with roll of the roll rate as a percentage of the steady roll rate, for each configuration at multiple aileron angles and a velocity of 20 m s^{-1}**

Fig. 16 **The variation in the aerodynamic torque about the centre of the numerical model with a flare angle of 10 degrees when it is held constant at varying roll angles and velocity**

vertically down. In steady flight the aerodynamic and gravitational forces balance, leading to non-zero coast angles. Thus, for a symmetric wing at zero AoA and zero roll, a FFWT will 'droop' as shown in configuration A in Fig. 16. In this configuration, assuming the centre of pressure and mass are coincident, the lift force acting on each wingtip is equal to the gravitational component perpendicular to the wingtip. Therefore the total vertical force transmitted through the hinge can be approximated as

$$F = \sin^2(\theta)\, m_f\, g \tag{14}$$

which for small fold angles will always be negative, creating a negative rolling moment. At a roll angle of zero degrees the forces acting on each wingtip are symmetric and hence the additional torques cancel.

However, at a non-zero roll angle the orientation of the gravitational forces changes in the reference frame of the FFWTs, changing the effective moment arm and hence the magnitude of the moment about each hinge. This gravitational moment will be at a maximum when the orientation of the wingtip is perpendicular to the gravitational acceleration, and a minimum when it is parallel. Considering configuration B in Fig. 16, it is important to note the orientation of the left and right wingtips are out of phase, with the right wingtip being horizontal in this configuration and the left just off vertical. In this state, the right wingtip does not produce a rolling torque and the left produces a torque which acts to increase the roll angle. As shown in Fig. 16, the differential between these two torques varies across all roll angles and always acts to move the wing towards the vertical position. This difference means that a wing with drooping FFWTs is unstable in roll and would require an aileron input to maintain a steady non-zero roll angle.

The scale of this instability is proportional to the steady-level coast angle. As shown in Fig. 16, as the velocity is increased the size of this differential torque reduces. This effect is because with increasing velocity the coast angle tends to zero, reducing the phase shift between the orientation of the left and right wingtip. Furthermore, at a coast angle of zero the wing would be neutrally stable and at negative fold angles, which could be achieved by adding camber to the wingtips, the phase shift would flip and the system would become stable in the horizontal position.

Considering once again a wing at a non-zero roll rate, the fold angle of each folding wingtip is a psuedo superposition of the mean response (which is driven by the zero-moment-angle and the centrifugal forces) and the variations due to gravity presented in Fig. 16. Gravitational variations act to accelerate the wing between 0 and 90 degrees roll and decelerate from 90 to 180 degrees, with the process repeating in the second half of the rotation. This effect explains the majority of the variations seen Figs. 14 and 15. There is however a phase shift present in these results, with the peak roll rate occurring beyond 90 degrees roll angle.

In the steady roll region, Fig. 17 shows how the fold angle and absolute orientation of the right wingtip varied for a flare angle of 10 degrees, aileron angle of 14 degrees and a velocity of $20\,\mathrm{m\,s^{-1}}$ in both the simulated and experimental case. In Fig. 17 the wingtip starts at A and then moves through B, C, D and E before returning to A, with an orientation of +90 degrees corresponding to the wingtip pointing vertically up and −90 vertically down.

16
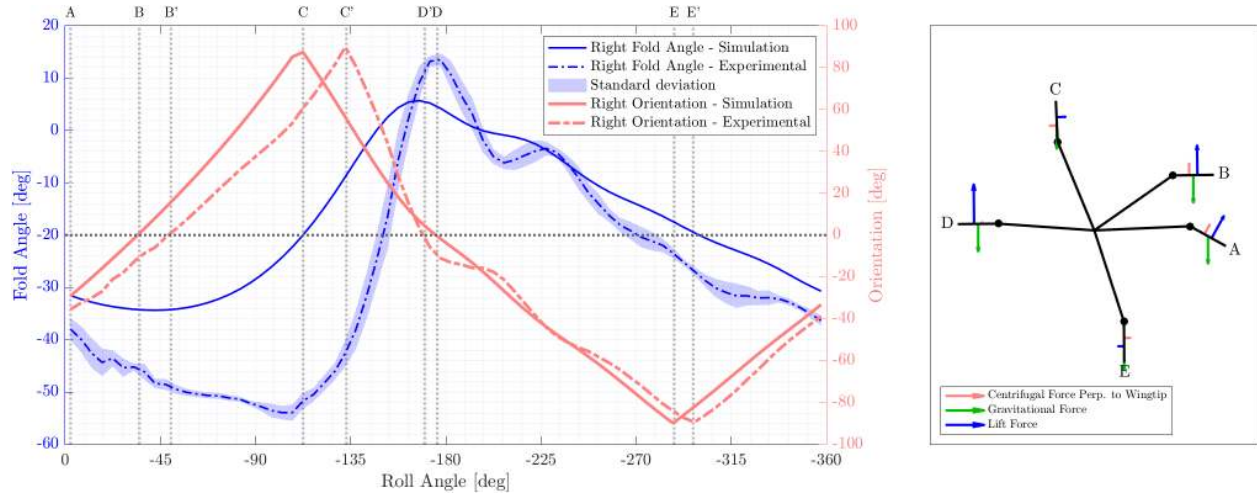
Fig. 17   On the left, the simulated and experimental variation of the fold angle and absolute orientation of the right wingtip during the steady roll rate region for a flare angle of 10 degrees, aileron angle of 14 degrees and a velocity of $20\,\mathrm{m\,s}^{-1}$. On the right, the position of the right wingtip at locations A thru E.

In Fig. 17 the orientation of the FFWT clearly follows a similar pattern to that described in Fig. 16, but as the zero moment angle acts to lag the motion of the inner wing the phase shift between the left and right wingtip is increased and the two neutral points (A and D in Fig. 16) are shifted to larger roll angles, which explains why the peak roll rate in Figs. 14 and 15 occurs beyond 90 degrees roll. As shown in Fig. 17 the story is similar in the experimental data, however as the mean fold angles were larger (Fig. 11) the neutral points are shifted to higher roll angles which increases the phase shift seen in Fig. 15. Another key point that can be taken from Fig. 17 is that between points C and D there is a rapid change in the fold angle which excites the 'pendulum' mode of the wingtip leading to the oscillations seen between D and E.

The relative magnitudes of the aerodynamic, inertial and gravitational forces determine the scale of the variations seen with respect to the roll angle of the model. These variations in the fold angle with respect to the roll angle, velocity and aileron angle, for both the numerical and experimental results can be seen in Figs. 18 and 19. At low speeds and low roll rate rates gravitational forces dominate, hence, the largest variations in both fold angle and steady roll rate are seen at the lowest wind tunnel velocity and aileron angle. In these conditions, the magnitude of the variations is up to approximately ±25% of the steady roll rate, with the majority of this variation being seen between ±60 deg roll. Therefore, depending on how the forces scale, gravitational forces may affect the roll performance of typical aircraft at low speeds, such as at take-off.

Increasing the flare angle increases the derivative of the aerodynamic forces with respect to the fold angle (e.g. larger flare angles require less change in the fold angle to counter the centrifugal and gravitational forces). As such, the variations in the fold angles with roll (and hence the roll rate) decrease with increasing flare angle. In a similar fashion, increasing the velocity also increases the aerodynamic derivative, reducing the variations seen in both the fold angle and the roll rate, as seen in Figs. 14 and 18.
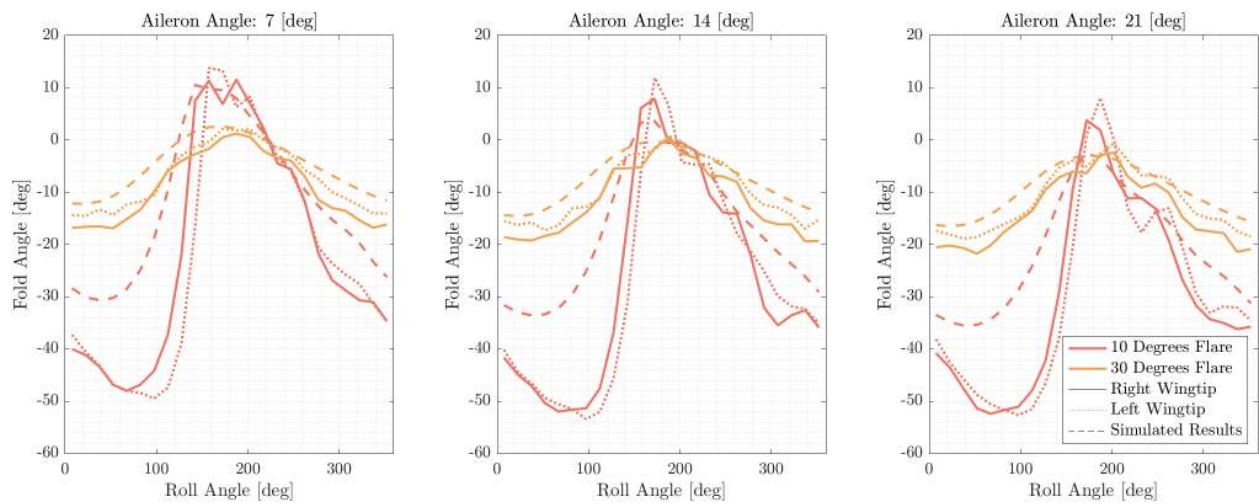
B. Roll Acceleration

Equation 6 shows the exact solution for the rolling motion of a fixed wing. In the *roll acceleration* region, the total torque about the centre of the wing decreases with roll rate due to the increase in aerodynamic roll damping. In the acceleration versus velocity phase space Eqn. 6 represents a straight line with a peak acceleration at zero roll rate, decaying to zero at the p_s. However, as can been seen in Figs. 9 and 20, the initial acceleration of the experimental model was heavily damped. The cause of which is believed to be the time taken for the electromechanical brake to fully release, altering the jerk of the model.

By altering the parameter τ_0 in Eqn. 12 the jerk of the numerical simulation could be tuned to that of the experimental data, with the effect of altering this parameter being shown in Fig. 20. By utilising the tuned value of $120\,\mathrm{ms}$ the phase space of each configuration could be directly compared, as shown in Fig. 21.

When comparing the fixed and removed case in Fig. 21, and recalling the aileron torque applied to each model is

17
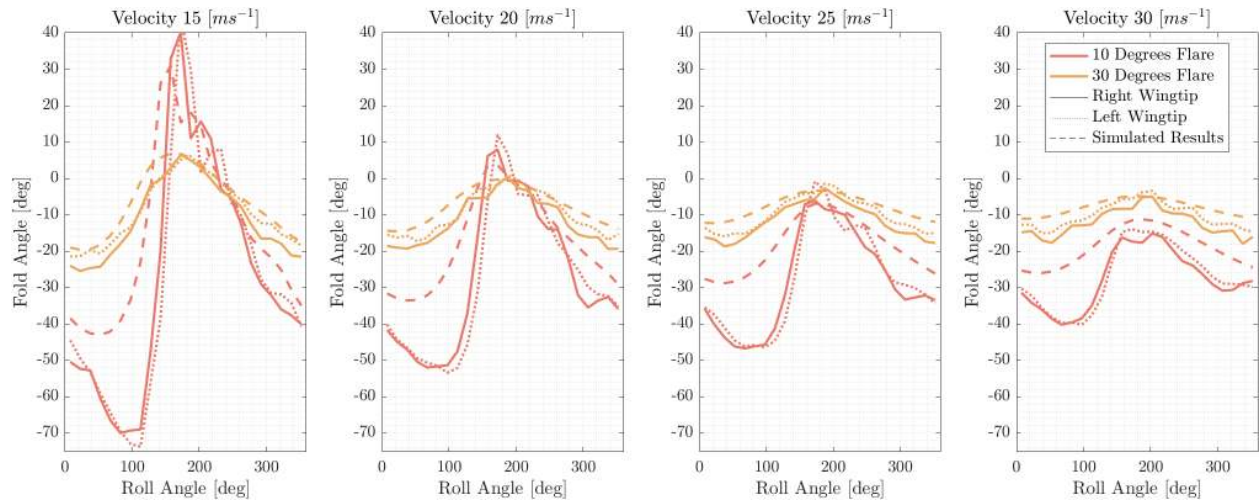
Fig. 18 Variation of the left and right fold angle with roll, for each configuration at multiple velocities and an aileron angle of 14 degrees
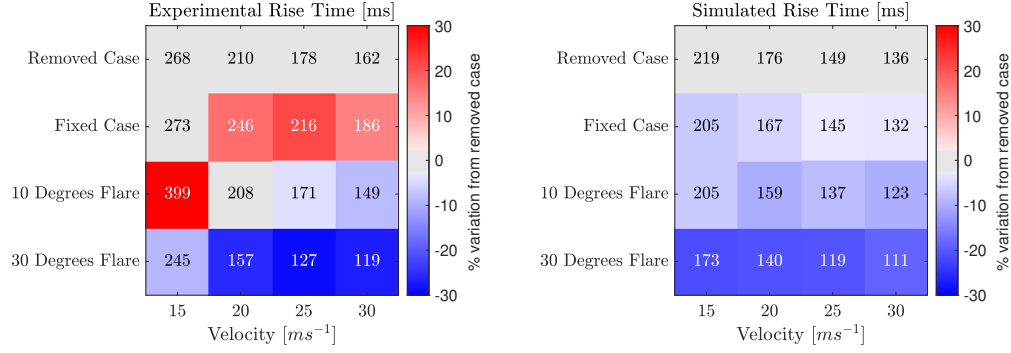

Fig. 19 Variation of the left and right fold angle with roll, for each configuration at multiple aileron angles and a velocity of 20 m s^{-1}
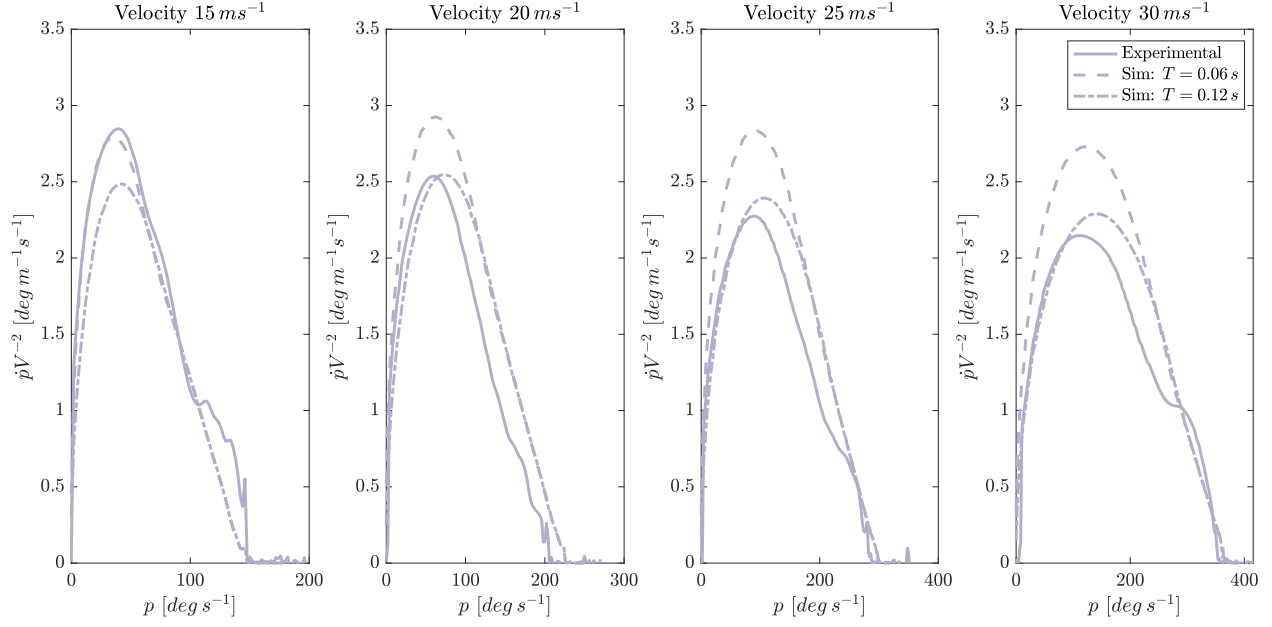
Fig. 20   A comparison of the experimental and simulated acceleration, velocity phase space for the removed case.
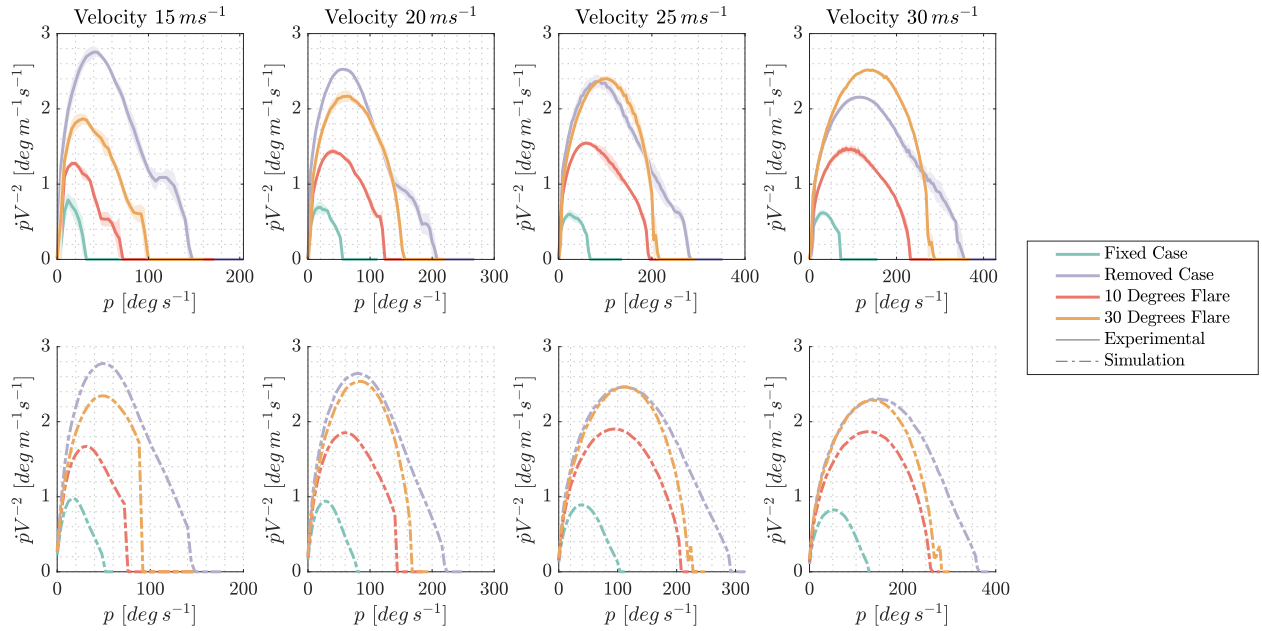
Fig. 21   A comparison of the experimental and simulated acceleration, velocity phase space for the each configuration

Fig. 22 A comparison of the average time constant for each configuration at each velocity, across all aileron angles

approximately the same, the increased inertia of the fixed case reduces the peak acceleration (the increased span also increases aerodynamic roll damping reducing the steady roll rate). Regarding the acceleration of the free cases, at low roll rates the inclusion of FFWTs increases the peak acceleration when compared to the fixed case, which has a similar inertia. Equally, the peak normalized acceleration grows with velocity and flare angle, and for the 30 degree hinge case grows to match or exceed the acceleration of the removed case. This growth in the normalised acceleration reduces the length of time required to reach the steady roll rate.

Considering again the solution to the simplified equations of motion (Eqn. 6), the time constant (T) is defined as the time taken for a system to reach 63.2% of the steady state value. Visually, this can be seen from Eqn. 6 to be

$$T = \frac{I_{xx}}{\tau_r} \tag{15}$$

By assuming the major component of the response of a wing with FFWTs is that of a first order system, we can estimate the time constant for each test case by measuring the time taken to reach 63.2% of the steady state value, with the results shown in Fig. 22. In general the free cases have a lower time constant than that of the fixed and removed case, with the exception of the slowest speed in the experimental data.

As before, these variations are due changes in the fold angle of the FFWTs. When the roll rate of a wing changes an additional inertial force ($F_{\dot{p}}$) emerges in the reference frame of the folding wing tip. This inertial force acts tangentially to the wingtip, moving it to a fold angle that lags the motion of the wing, changing its local AoA in such a way as to produce a force which aids the rolling motion of the wing.

In the previous sections all analysis has assumed the system is in a pseudo steady state, and the response of the wingtip is fast enough so that changes to the fold angle, such as due to gravity, happen instantaneously. However, in the case of roll acceleration, the dynamics of the FFWT must also be considered. During the roll acceleration region the equilibrium position of each wingtip is constantly changing. How each wingtip reacts to this is dependent on the frequency and damping of the flapping motion of the wingtip.

Figure 23 shows the time history of the roll rate and left and right fold angles for a flare angle of 30 degrees and a velocity of $25\,\text{m}\,\text{s}^{-1}$. In this figure the steady-roll-region values are also shown as dashed lines and correspond to the value at a current roll angle. e.g. if at $100\,\text{ms}$ the roll angle was 15 degrees the dashed line represents the roll rate and fold angles at 15 degrees in the steady-roll-region (shown in Figs. 18 and 14)

From Fig. 23 it can be clearly seen that both the experimental and simulated fold angles move away from the initial coast angle and oscillate about the mean value. In regions where the fold angle lags the mean value (more positive for the right wingtip and more negative for the left) the roll acceleration is enhanced, and when they lead the mean value it is reduced. Over time these oscillations damp out with the values tending to those of the mean.

Figure 24 shows the results for a flare angle of 10 degrees at a velocity of $20\,\text{m}\,\text{s}^{-1}$. Comparing the simulated data to that of the 30 degrees case shows a similar pattern, with the fold angle moving towards and then oscillating about the values of the steady-state region. Visually, the response of the 10 degrees case is slower, meaning that the wingtips provide less 'roll acceleration assistance' during the primary acceleration phase. This response time is dependent on the natural frequency of the wingtips flapping mode, which for small fold angles has been previously shown to be proportional to [6]
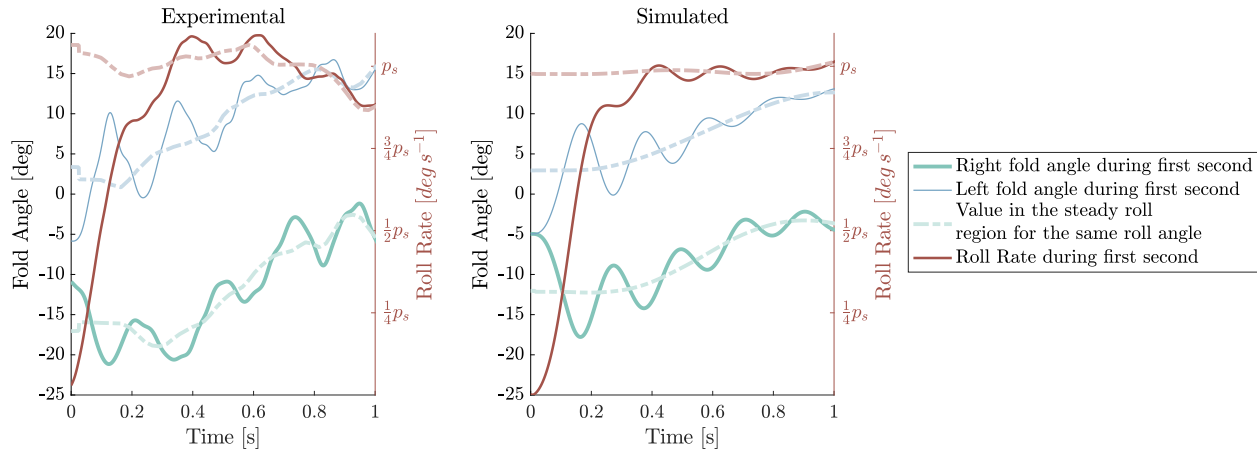
Fig. 23   A comparison of the simulated and experimental response in the roll acceleration region of the left and right wingtip with a flare angle of 30 degrees, at a velocity of $25\,\mathrm{m\,s^{-1}}$ and an aileron angle of 14 degrees
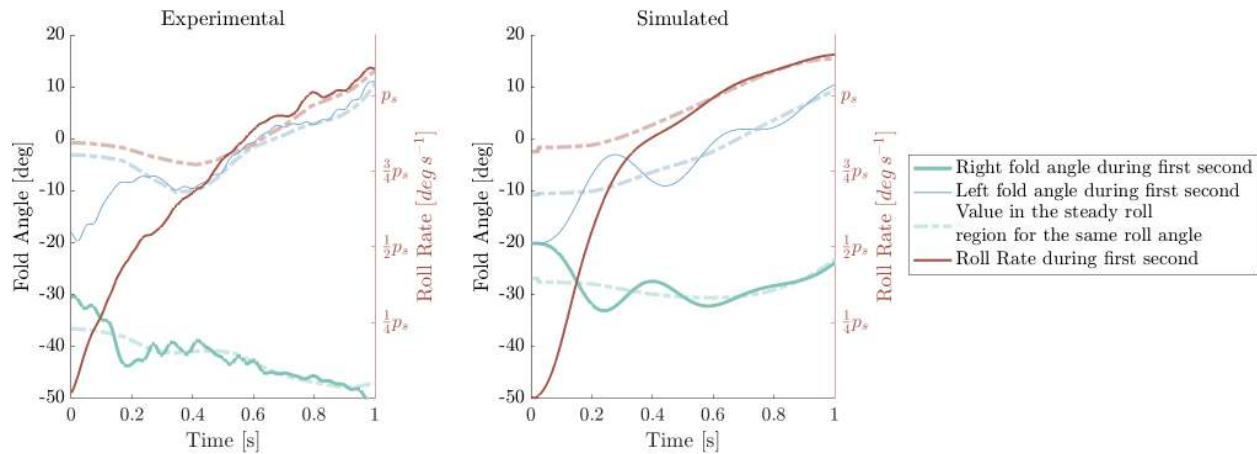
Fig. 24   A comparison of the simulated and experimental response in the roll acceleration region of the left and right wingtip with a flare angle of 10 degrees, at a velocity of $20\,\mathrm{m\,s^{-1}}$ and an aileron angle of 7 degrees
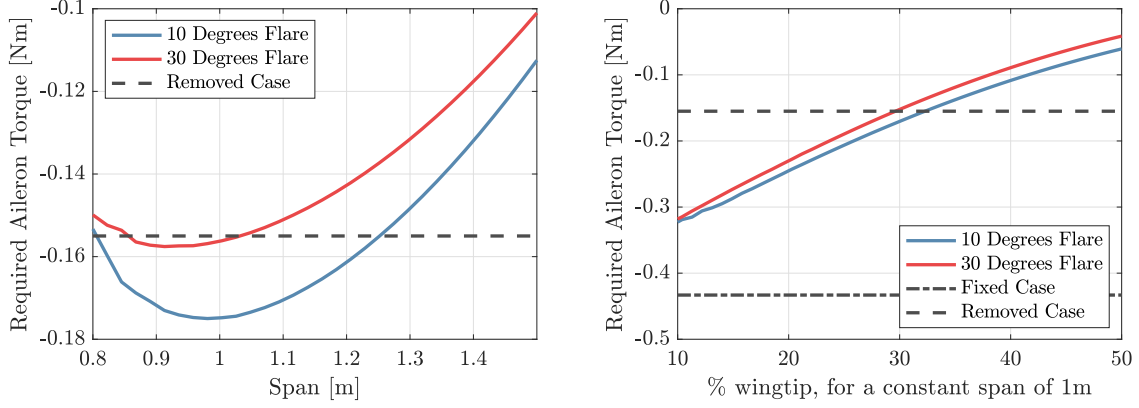
Fig. 25 **The variation in the required aileron torque to maintain a roll rate of $60 \deg s^{-1}$ at zero roll angle and an airspeed of $25\,m\,s^{-1}$ as a function of a) span, with the hinge line at $728\,mm$ b) Sigma - The ratio of the total span that is folding wingtip, for a constant total span of 1m**

$$f \propto V \sqrt{\frac{\sin \Lambda (1 - \xi_n^2)}{I_{xx}}} \tag{16}$$

where ξ_n is the modal damping. From this expression it can be concluded that larger flare angles and higher velocities will increase the frequency and therefore the response time of FFWTs, reducing the time constant of the model. This trend is clearly seen in Fig. 22.

In Fig. 24 the experimental response is significantly damped, which both reduces the frequency of the FFWT mode and prevents the fold angles from oscillating about the mean values in the *steady roll* region. This effect results in significantly less 'roll acceleration assistance' from the FFWTs, increasing the time constant of the model, as is seen at the lower speeds in Fig. 22. The source of this additional damping is currently under investigation.

## VI. Further Discussion and Implications for Civil Aircraft

For a typical aircraft configuration, increasing the wingspan leads to slower roll acceleration and lower steady roll rates, making an aircraft significantly less manoeuvrable. The results in the previous section have shown that FFWTs can significantly reduce the aerodynamic roll damping and increase the transient roll acceleration of the described wind tunnel model. However, what does this mean for other configurations and how does this scale to more typical aircraft?

Many of the geometric properties of the rig used in the experimental model were held constant. However, many of the results indicate altering the geometry of the wingtip may further increase the roll performance of model.

Regarding the length of a wingtip, recall in Fig. 12, which only considers aerodynamic force, the forces acting on a wingtip at a constant roll rate can be categorized into two regions. Region 2 aids the rolling motion whereas region 3 counters it. As the moments of region 2 and 3 balance and region 2 is closer to the hinge, the magnitude of the force applied in region 2 must be higher than that of region 3. Therefore, as only shear forces are transmitted through the hinge, a FFWT has a net negative contribution to roll damping.

Next, consider extending the wingtip slightly. This change increases the size of region 3, so to balance the moments about the hinge the zero-moment-angle must change, increasing the size of region 2 by a greater amount due to its proximity to the hinge. As only shear forces are transmitted across the hinge, the net contribution of the extended wingtip to aerodynamic roll damping must therefore decrease. This leads to the counter intuitive conclusion that when aerodynamic forces dominate (such as at low roll rates) increasing the span of the wingtip will increase the aerodynamic roll damping alleviation of FFWTs.

This point is illustrated in Fig. 25, where the aileron torque required to achieve a steady roll rate of $60 \deg s^{-1}$ for wings of different spans is shown. In these simulations the distance between the centre of rotation and the hinge line remains constant, with the length and mass of the FFWTs growing with the change in span. From this figure there is a clear trend that longer wingtips increase the steady roll rate, with both flare angles matching the performance of the removed case by a span of $1.25\,m$.

22
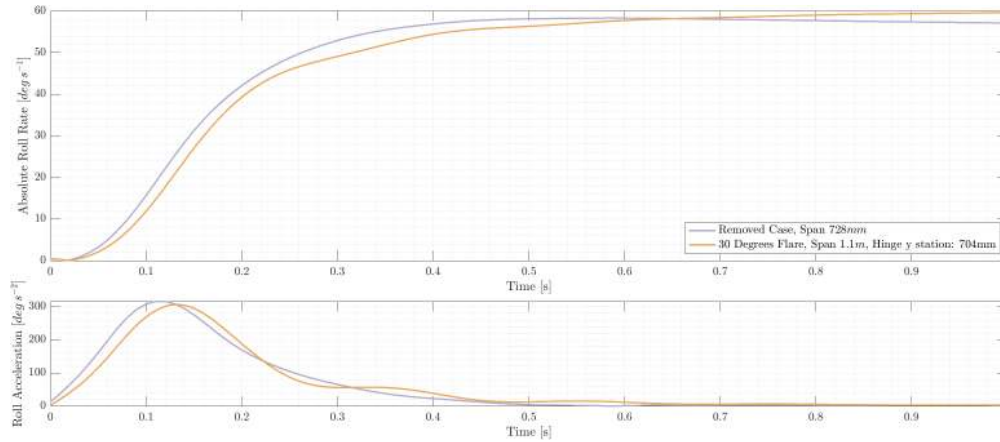
Fig. 26   Example numerical time traces for the removed case, and a wing of span 1.1 m with a flared folding wingtip with flare angle 30 degrees, and a hinge position of 682 mm at $25\,\mathrm{m\,s^{-1}}$ and an aileron angle of 3 degrees

The performance can be further enhanced by moving the hinge line inboard. This change decreases the size of region 1 in Fig. 12, reducing the aerodynamic roll damping. Fig. 25 shows the effect of moving the hinge line for a constant span of 1 m, showing once again the performance of the removed case can be achieved with a relatively modest change in the ratio of FFWTs.

By selecting a wing span of $1.1m$, a flare angle of 30 deg, and a hinge position of 704 mm, the transient response of an 'optimised' FFWT can be compared to that of the removed case, as shown in Fig. 26. The aileron angle in these simulations was chosen to achieve an approximate mean steady roll rate of $60\,\mathrm{deg\,s^{-1}}$. As shown in Fig. 26 the same roll rate as the removed case can be achieved by altering the geometry of the wingtips.

In the first phase of the roll acceleration region the 'optimised' wingtip lags behind the removed case as the wingtips take time to move to a position in which they aid the motion, whereas in the second phase the 'optimised' wingtip continues to accelerate, eventually surpassing the roll rate of the removed case. This highlights the importance of the natural frequency of the wingtips when compared to that of the rolling motion.

As shown in this simplified analysis, the roll performance of a wing incorporating FFWTs can be significantly altered by modestly changing the basic geometry of the wingtip, even achieving performance beyond that of the removed case. By further assessment of the design space, such as applying twist to the wingtips to tailor the forces in regions 2 and 3 of Fig. 12, it is conceivable that FFWTs could be used to increase the total wingspan of an aircraft whilst maintaining the same, if not better, roll authority as that of the original span.

However, when compared to a conventional fixed wing aircraft additional considerations are required when assessing the performance of a wing incorporating FFWTs:

- The roll stability of an aircraft incorporating FFWTs is a function of both the coast angle and its attitude, with drooping coast angles reducing the roll stability of an aircraft. Therefore, it is possible that large variations in the stability of an aircraft may occur across different phases of a flight, and thus care will be required to understand what the limiting cases may be.
- The roll performance of an aircraft incorporating FFWTs is a function of the instantaneous roll angle. Hence maneuvers of an equal magnitude (such as 0 to 30 degrees roll and -15 to 15 degrees roll) may not have identical responses. Therefore, additional care is required when selecting the critical design cases for such a system.
- In the roll acceleration phase region, the oscillatory motion of the FFWTs can induce significant oscillations in the roll rate of the aircraft,as seen in Fig. 23. The frequency and magnitude of these oscillations will vary with airspeed and aircraft attitude meaning an aircraft may have significantly different handling qualities at different parts of the flight envelope.

VII. Conclusions

To increase the overall aerodynamic efficiency of future aircraft designs there is a push within the industry to increase the wing span, and therefore aspect ratio, of the next generation of aircraft. This increase in aspect ratio reduces the induced drag, improving the overall efficiency. However, this increase in span comes with additional issues such as

supporting the larger bending moment at the root, interfacing with the current infrastructure at airports, and maintaining sufficient control authority of the aircraft. Flared folding wingtip (FFWT) devices have previously been shown to aid with the operational and structural requirements, with initial simulations suggesting they may improve the roll authority of an aircraft. In this paper a novel wind tunnel experiment was developed which validates the use of FFWTs to significantly improve the roll performance of an aircraft when compared to a fixed configuration of the same span. This improved roll performance is achieved by unloading the wingtip during roll, reducing the developed aerodynamic roll damping, thus increasing the maximum roll rate of the aircraft. Furthermore, FFWTs have been shown to increase the peak angular acceleration of a wing, reducing the time taken to establish a steady roll rate, further improving an aircraft's roll performance. These results have been compared to steady and transient numerical simulations of a simple 3 DoF system, with good correlation being seen between the two data sets. By further exploration of the design space with this numerical model, it has been shown that FFWTs could be used to increase the total wingspan of an aircraft whilst maintaining the same, if not better, roll authority as that of the original span.

Acknowledgments

References

[1] Anon., "Aircraft Technology Roadmap to 2050," Tech. rep., IATA, 2019.

[2] "Carbon Offsetting and Reduction Scheme for International Aviation (CORSIA)," , 2020. URL https://www.icao.int/environmental-protection/CORSIA/Pages/default.aspx, [retrieved 2 June 2020].

[3] Castrichini, A., "Parametric Assessment of a Folding Wing-Tip Device for Aircraft Loads Alleviation," Phd. thesis, University of Bristol, UK, 2017.

[4] Castrichini, A., Hodigere Siddaramaiah, V., Calderon, D. E., Cooper, J. E., Wilson, T., and Lemmens, Y., "Nonlinear Folding Wing Tips for Gust Loads Alleviation," *Journal of Aircraft*, Vol. 53, No. 5, 2016, pp. 1391–1399. https://doi.org/10.2514/1.c033474.

[5] Cheung, R. C. M., Rezgui, D., Cooper, J. E., and Wilson, T., "Testing of a Hinged Wingtip Device for Gust Loads Alleviation," *Journal of Aircraft*, Vol. 55, No. 5, 2018, pp. 2050–2067. https://doi.org/10.2514/1.c034811.

[6] Castrichini, A., Siddaramaiah, V. H., Calderon, D. E., Cooper, J. E., Wilson, T., and Lemmens, Y., "Preliminary investigation of use of flexible folding wing tips for static and dynamic load alleviation," *The Aeronautical Journal*, Vol. 121, No. 1235, 2017, pp. 73–94. https://doi.org/10.1017/aer.2016.108.

[7] Dussart, G., Yusuf, S., and Lone, M., "Identification of In-Flight Wingtip Folding Effects on the Roll Characteristics of a Flexible Aircraft," *Aerospace*, Vol. 6, No. 6, 2019, p. 63. https://doi.org/10.3390/aerospace6060063.

[8] Wilson, T., Castrichini, A., Azabal, A., Cooper, J., Ajaj, R., and Herring, M., "Aeroelastic Behaviour of Hinged Wing Tips," *Int Forum Aeroelasticity and Structural Dynamics*, 2017.

[9] Castrichini, A., Wilson, T., Saltari, F., Mastroddi, F., Viceconti, N., and Cooper, J., "Aeroelastics Flight Dynamics Coupling Effects of the Semi-Aeroelastic Hinge Device," *Journal of Aircraft*, 2019, pp. 1–9. https://doi.org/10.2514/1.C035602.

[10] Cheung, R. C. M., Rezgui, D., Cooper, J. E., and Wilson, T., "Testing of Folding Wingtip for Gust Load Alleviation of Flexible High-Aspect-Ratio Wing," *Journal of Aircraft*, 2020, pp. 1–13. https://doi.org/10.2514/1.c035732.

[11] Anon., "Part 23 - Airworthiness standards: normal, utility, acrobatic, and commuter category planes," 14 c.f.r., Federal Aviation Regulations, 2020.

[12] Anon., "Certification Specifications and Acceptable Means of Compliance for Large Aeroplanes," Cs-25, EASA, 2019.

[13] Meurer, A., Smith, C. P., Paprocki, M., Certík, O., Kirpichev, S. B., Rocklin, M., Kumar, A., Ivanov, S., Moore, J. K., Singh, S., Rathnayake, T., Vig, S., Granger, B. E., Muller, R. P., Bonazzi, F., Gupta, H., Vats, S., Johansson, F., Pedregosa, F., Curry, M. J., Terrel, A. R., Roucka, S., Saboo, A., Fernando, I., Kulal, S., Cimrman, R., and Scopatz, A., "SymPy: symbolic computing in Python," *PeerJ Computer Science*, Vol. 3, 2017, p. e103. https://doi.org/10.7717/peerj-cs.103.

[14] "Aerosandbox," , 2020. URL https://peterdsharpe.github.io/AeroSandbox/, [retrieved 27 October 2020].

[15] Murray, R. M., *A Mathematical Introduction to Robotic Manipulation*, 1st ed., Routledge, 1994.